A scalable, light-controlled, individually addressable, non-metal actuator array

Sophie Paul^{1*}, Matthew R. Devlin¹, and Elliot W. Hawkes¹

Abstract—Research in the area of photo-actuation is growing rapidly, yet there are few examples of photo-actuators with practical use cases. One potential application is for the control of intelligent electromagnetic surfaces, or two-dimensional arrays that could shape and control an incident electromagnetic field in ideally any manner. A promising concept to realize such a surface leverages signal refraction via antenna edges, but requires non-metal actuation, large antenna rotations, and high antenna angular accuracy for long periods of time. Here, we present a nonmetal, light-controlled, multi-position inchworm actuator array that can rotate an antenna 88 degrees in incremental steps of less than 3.4 degrees with zero-power shapepersistence. The design is modular and rapidly manufacturable via a layered laser-cutting technique, such that the actuator can be tiled into an array to control the rotation of many antennas. We control the array with a single focused IR light that rasters across the actuators to precisely control all antenna positions. We characterize the response time, accuracy, and repeatability of a single actuator, and demonstrate the array achieving diverse antenna configurations. This work advances the precision and scalability of photothermal actuation not only for use in intelligent electromagnetic surfaces but for any application benefitting from light-controlled actuation.

I. Introduction

The conversion of light into mechanical work, either directly, via the photomechanical effect, or indirectly through heat, via the photothermal effect, is a rapidly growing area of research [1], [2], [3]. However, much of this work has focused on improving chemistry and material properties for improved performance without direct application to engineering problems. In this work, we seek to address a challenge in the area of antenna array design for which photoactuation is uniquely well-suited.

Specifically, we consider the field of communication systems, in which the ultimate goal is to provide reliable high-speed connectivity for all the users. With the number of connected devices predicted to reach 500 billion by 2030 [4], next generation communication systems face unprecedented challenges to meet the demand. In this context, intelligent electromagnetic (EM) surfaces have gained considerable attention in both academic and industry in recent years [5], [6], [7], [8], [9], as they are promising contenders for the enhancement of 5G communication networks and enabling novel 6G system designs [2]. Further, intelligent EM surfaces could benefit applications such as creating smart radio environments, localization, security, and privacy [10]. However, most efforts in the area of intelligent EM surfaces

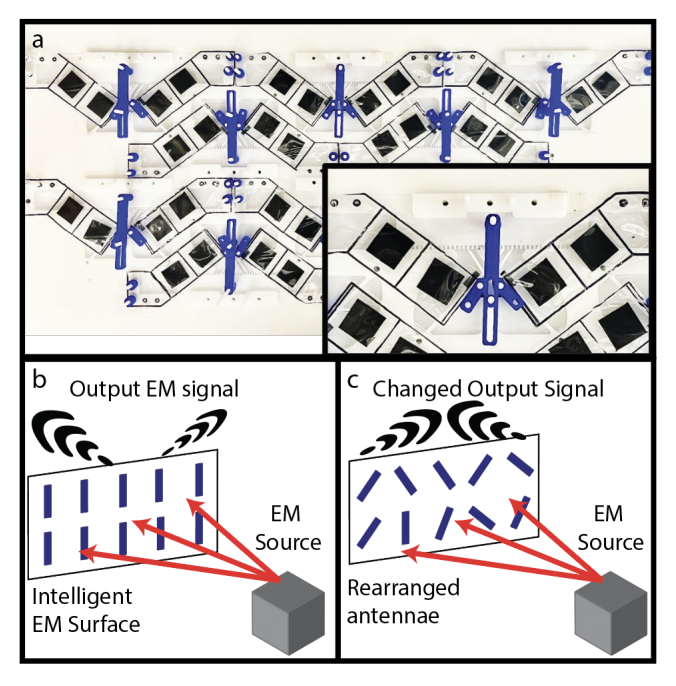


Fig. 1: a) Fabricated light-controlled, non-metal actuator array of 10 units. Inset photo is of one unit. b-c) Schematic of possible application as a reconfigurable EM surface.

have been theoretical or have only demonstrated focusing of the field at a single point. A few studies have shown focusing at two points, and fewer up to four [11]. However, these designs all require complex and expensive unit designs. In contrast, promising recent work shows the ability to reradiate energy simultaneously in multiple directions using low-cost everyday materials and commodity transceivers, by exploiting diffraction off of the array [11].

The key next step for this work is to advance from manually placed static array elements to a robotically controlled system. To enable this, however, there are challenging design requirements. The actuating array cannot have metal components, which would disrupt the signal. Yet at the same time, the array must be able to move the 3-cm antennas through a large range of angles, hold them stably in positions for long periods of time, and control the position of all antennas with high resolution.

The first requirement of non-metal actuation leads to the possibility of photoactuation, since many of the previous works show metal-free movement. For instance, Liquid Crystal Elastomers (LCEs) are polymers that exhibit a reversible phase change when heated above a certain transition temperature to create large strains (e.g., [12], [13]). Both Azobenzene [14] and CNTs [15] are used as photothermal agents to actuate LCEs. However, these actuators require

This work is supported in part by the National Science Foundation grant 1935327.

¹Department of Mechanical Engineering, University of California, Santa Barbara, CA 93106.

^{*} Corresponding author. Email: s_paul@ucsb.edu

specialized equipment and processing.

An alternative class of photoactuation with a much simpler fabrication and materials is photothermal phase change actuation. One example is the use of Novec 7000, which exhibits a large expansion when changing phases from liquid to gas, enclosed in a pouch that contains a photothermal absorber to convert applied light into heat [16]. These pouch motors inflate upon heating as the fluid expands into a gas. This inflation can be used to push, or the lengthwise contraction can pull, as traditional pouch motors powered by compressed air [17]. However, it is very challenging to achieve high accuracy and repeatability with photothermal pouch motors, since the actuation has a highly non-linear response to the input light, and requires continued light input to maintain a position.

Thus to meet our design requirements, we looked toward an inchworm actuation mechanism to convert the motion of photothermal pouch motors into both large-range and high-accuracy rotation of the antennas. This technique has been leveraged by the Microelectromechanical Systems (MEMS) field to develop various stepping actuators [18]. For example, a micropositioning actuator that generates large displacements in discrete steps fabricated in silicon achieved a step size of 8 µm [19]. However, MEMS devices require advanced manufacturing techniques which limit the size to the micrometer scale [20].

Thus, to fulfill the design requirements of the intelligent EM surface application, we build upon the metal-free photothermal induced contraction of a pouch motor and the high position resolution of a ratcheting inchworm mechanism to create a new photoactuator. Specifically, we present a modular, centimeter-scale, non-metal, photothermal, multi-position inchworm actuator array that can move a hinge greater than 80 degrees in incremental steps of less than 3.4 degrees with locking capabilities. It is fabricated with a layered laser cutting technique that allows scalable manufacturing.

II. DESIGN CONCEPT

In this section, we propose the design of a non-metallic, modular, light-addressable actuator. We first discuss the design requirements, then an overview of the proposed design, and finally the details of the components of the design.

A. Design Requirements

Our design is driven by the key design requirements for the application of an intelligent electromagnetic surface (Table I). The first requirement is that all materials and actuators of the device must have low interference for signals passing through the antenna. Quantitatively, this means that everything in the device (besides the antenna flaps themselves) must have a dielectric permittivity constant below 5. Second, the array needs high accuracy and step resolution for antenna rotation. Specifically, a step size less than 3.4 degrees, and no farther than a single step off of target. Third, the antenna must be able to rotate across a large range, at least 80 degrees, or 40 degrees to each side. Fourth, a rotated antenna must hold its position even after stimulus removal. This angle

	Design Require-	Metric	Design Feature
	ment		
1	Low EM interfer-	Dieletric Permit-	PMMA and
	ence materials and	tivity Constant<5	Delrin parts;
	actuators	(no metal present)	Photothermal
			pouch actuators
2	Easily scalable (in	If n units requires	Laser cut entire
	number of units)	t time, then	array in once
		2n units must	piece
		require<2t time	
3	Antenna rotation:	Step size< 3.4	Inchworm
	High resolution	degrees[11]	mechanism with
	through large	through 0-40	small teeth and
	angle range	degrees of range,	large travel
		on each side	
4	Antenna rotation:	Holds within $+/-$	Cantilever tip de-
	Position retention	1 degree over 30	sign
	upon stimulus re-	seconds	
	moval		
5	High accuracy and	hit within $+/-1$	Linkage design
	repeatability	mm of target for	(size of teeth,
		every movement	angles, pivot
		of rack	locations, etc.)

TABLE I: Design parameters that guide the prototyping process

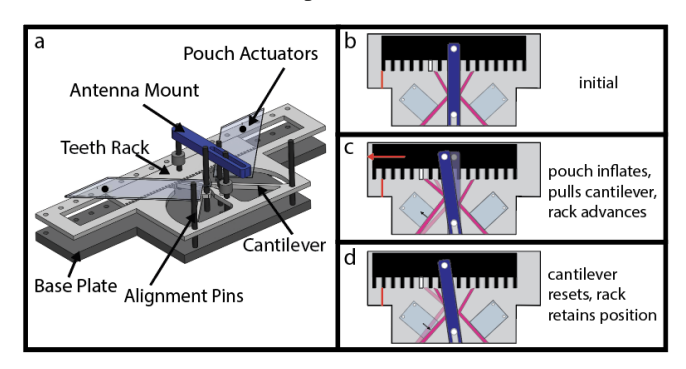


Fig. 2: a) One rendered unit (20 x 7.5cm) with all parts labeled, and b-d) a schematic demonstrating how to device moves the rack in both directions. A stimulus is applied to move the rack to the left a single step, then a second step, then the stimulus is removed. The position is retained.

must be held for at least 1 minute within a single degree of rotation. Lastly, the array must be scalable in both size and number of units. Ideally, we seek to have manufacturing time scale sub-linearly with number of units. For instance, we aim to have a 10x increase in the number of units to take less than 10x the amount of time to construct.

B. Design Overview

This section explains the design of the device and provide details on how each component of the device functions. At a high level, the device is an array that controls the individual orientation of many antennas (Fig. 1). Each antenna is mounted to a pivot and can rotate with one degree of freedom. This rotation is controlled by the lateral motion of a rack, which is in turn controlled by the motion of cantilevers, driven by photothermal actuators. A remote light powers the actuators. Once sufficiently heated, the left actuator pulls the left cantilever to advance the rack one step to the left. The opposite occurs for the right actuator. Critically, none of the parts of the unit are metallic.

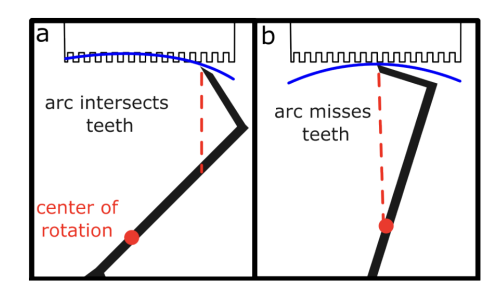


Fig. 3: Details of the cantilever design. a-b) Because there are two cantilevers for each unit (see Fig. 2), the inactive one must remain out of contact with the rack to allow the active cantilever to move the rack. Accordingly, the center of rotation of the cantilever must be offset from the tip to allow it to move vertically to engage the rack (a). A center of rotation below the tip results in the cantilever missing the rack (b).

1) Inchworm Mechanism: The inchworm mechanism has three primary components: the antenna mount, the rack of teeth, and two cantilevers. Most importantly, all parts of made of plastic, satisfying Design Requirement 1 in Table I.

The antenna mount is comprised of a long acrylic section with a hole on one end and a slot on the other. The hole allows the mount to pivot with respect to the rack, while the slot allows the hypotenuse to lengthen as it rotates. The friction of the press-fit on the pivot pin on the antenna holder allows for one-way motion without an accidental reset to the initial position (Design Requirement 4, Table I). This allows us to avoid the complexity of an active brake, as used in previous MEMS designs [19].

The rack and teeth are made from low friction Delrin, with carefully selected tooth pitch in order to determine resolution as will be later discussed in Fig. 4 (Design Requirement 3, Table I). The rack advances tooth by tooth, and this lateral motion relative to the base plate causes the antenna mount to rotate. A symmetrical rack allows for the device to have two cantilevers on either side ensuring bidirectional angle control. The length of the rack determines the total range of possible angles for the antenna, which is a total of 88 degrees in this prototype (Design Requirement 3, Table I).

The cantilevers flex when pulled by the photothermal pouch motors, allowing a single tooth to be caught and the antenna mount advanced by a single step. Fig. 3 shows the details of the swing of the cantilever; the functional center of rotation of the bending beam must be offset from the tip, so that it can move up and engage the rack during deflection. The angle of the cantilever tip design is critical to push the rack one direction, but slip during its return.

2) Photothermal Pouch Motors: Key to the design is its avoidance of metallic components (Design Requirement 1, Table I). This makes traditional means of actuation, such as servo motors, not feasible. Instead, we turned to a soft, photothermal actuator that can be controlled and powered remotely. Our design requires that the photothermal actuators have a specific stroke and contraction force in order to activate the inchworm mechanism, and a cycle time on the order of 10s of seconds. We explore the specifics of stroke,

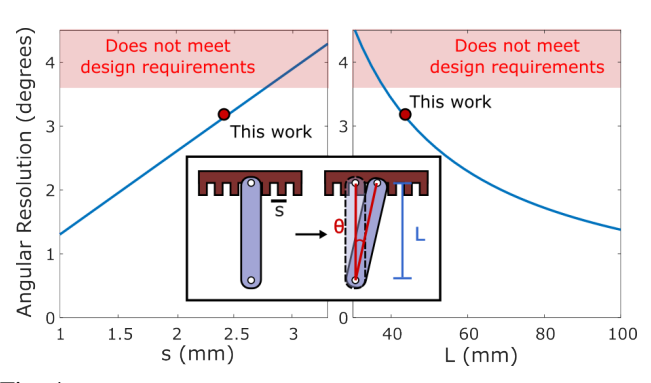


Fig. 4: The first model describes how geometric parameters of the design affect angular resolution. The shaded red region represents a region unacceptable by our design parameters in Table I. The red circle shows the parameters chosen for this work.

force, and thermal cycling times in Section III.

3) Modular Tiling: In order to tightly pack the units, we tile the units in alternating cantilever orientations. Additionally, the bulk of entire array is a single layer and can be laser cut in a single piece (Design Requirement 5, Table I). Additional sliding and rotating components are cut and added simply with press fit Delrin pins. While increasing the density of the array, we ensure that the pouch motors are carefully spaced to avoid crosstalk when targeting a specific photothermal actuator.

III. MODELING

In this section, we describe simple mathematical models that aid in the design of the proposed device. The models offer design insights for the mechanical design of the antenna mount, rack, and cantilever as well the design of the photothermal actuator to meet the force and displacement needs of the device.

A. Angular Resolution of Antenna Rotation

The first model is a tool for determining the angular resolution of the antenna movement within the proposed device. It takes into account tooth spacing, number of teeth moved per cycle, cycle number, and the distance between the rack and the pivot. This can offer a designer a tool for hitting a specific resolution they need. This model is:

$$\theta_{n+1} - \theta_n = \arctan\left[\frac{(n+1)s}{L}\right] - \arctan\left[\frac{ns}{L}\right] = \Delta\theta$$
 (1)

Where θ_{n+1} is the new cantilever angle after a single cycle step, θ_n is the current cantilever angle, n is the cycle number, s is the step size, and L is the length between the rack and the pivot (Fig. 4, insets). The model can be further visualized in Fig. 4 which relates the parameters back to the design parameters in Table I. The red shaded region in Fig. 4 is unacceptable per our design requirements, and the selected values for manufacture are represented by the red circle.

The model also describes how the step size slightly changes with the rack position. The relationship is non-linear, so it is important for use to have the model on hand to know exactly how many steps are required to reach a target antenna angle. (See Fig. 9 for this relationship.)

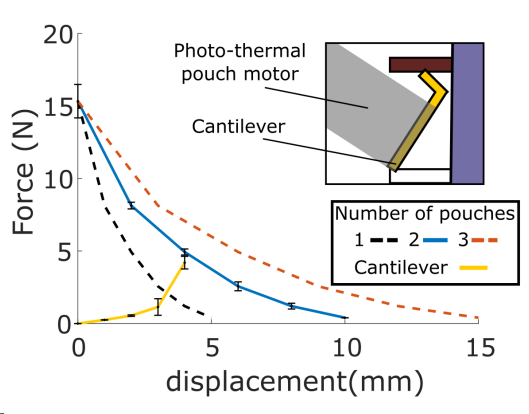


Fig. 5: The second model describes the relationship between the forces and displacements produced by pouch motors compared to that required to move the cantilever. Using experimentally measured curves, the model suggests that that at least 2 pouches in series are required.

B. Cantilever Stroke and Pouch Contraction

The second model informs the design of the pouch motor based on a selected cantilever design. We compare the forces of the actuator and cantilever:

$$F_{act}\left(\frac{x}{n_p}\right) > F_{cant}\left(x\right), \left\{x_i \le x \le x_f\right\} \tag{2}$$

where F_{act} is the force exerted by the photo-thermal pouch motor, x is the cantilever displacement, n_p is the number of pouches in series, F_{cant} is the force to move the cantilever, x_i is the initial position of the cantilever, and x_f is the maximum possible displacement of the cantilever.

Both F_{act} and F_{cant} are nonlinear and nontrivial to model. F_{cant} initially behaves according to Euler-Bernoulli beam theory, however becomes nonlinear due to interactions with the rack. F_{act} also does not follow the simple geometric model outlined in [17] due to the thickness of the multi-layer mylar. Thus, we use Eq. 2 with empirical data, shown in Fig. 5 to determine that two pouches are necessary to satisfy the force and displacement requirements of this mechanism.

C. Thermodynamics of Pouch Motors

The third model describes the heating and cooling of the photothermal pouch motors and offers design guidelines for the necessary power for the actuating light, derived from [21]:

$$t_{heating} = \left(\frac{E_t}{P - hA(\Delta T)}\right) \tag{3}$$

where $t_{heating}$ is the time to heat a pouch, E_t is energy required to heat Novec 7000 from 25C° to 34C°, P is the input power into the system, h is the convection coefficient, A is the pouch area, and ΔT is the temperature difference between the pouch and the surroundings. The model is visualized in Fig. 6, and shows that input power on the order of 5 W is required for the range of h values explored.

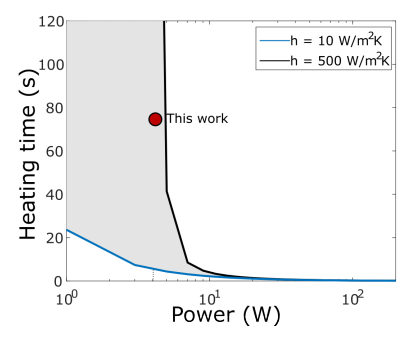


Fig. 6: The third model describes the thermodynamics of heating a pouch. The model suggests that for the expected range of convection coefficients, *h*, [21] heating will take on the low end around 4 seconds and on the high end 40 seconds for 5 Watts input power.

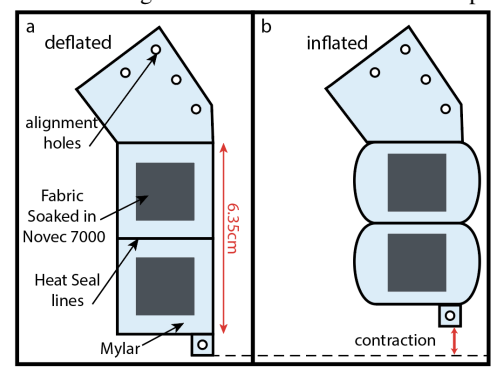


Fig. 7: Schematic of the pouch actuators. Each actuator has two pouches in series to enable sufficient stroke. a) pouch actuator deflated, b) inflated and contracted pouch actuator (not to scale).

IV. FABRICATION

In this section, we give an overview of the manufacturing process for the two main components of the design, the array of inchworm mechanisms and the photothermal pouch motors. Importantly, this section describes how the choice of materials and manufacturing processes allows us to satisfy Design Requirements 1 and 2 from Table I.

A. Inchworm Mechanism

The mechanism is constructed by stacking laser cut pieces in 3 layers and held in place with alignment pins, as shown in Fig. 7. The first layer is the base layer and holds everything together. The next layer includes the frame with the cantilevers and the rack. Then, the photothermal pouch motors are pinned to the cantilevers and the edge of the unit, with spacers on top to hold them in place. Lastly, the antenna mount is pinned to the rack and main body. The design allows for the entire array to be fabricated in one cut (for each layer), including as many units as can fit in a given laser cutter. Due to the tiling scheme, each marginal unit does not require as many cuts as the first unit. Thus, fabricating 10 units takes 80 minutes, but cutting the 10-unit array in one cut takes only 55 minutes. This satisfies Design Requirement 2, Table I.

B. Novec-filled Pouch Motors

To fabricate the pouch motors, we followed a procedure adapted from [16],[17].The pouch motors were fabricated

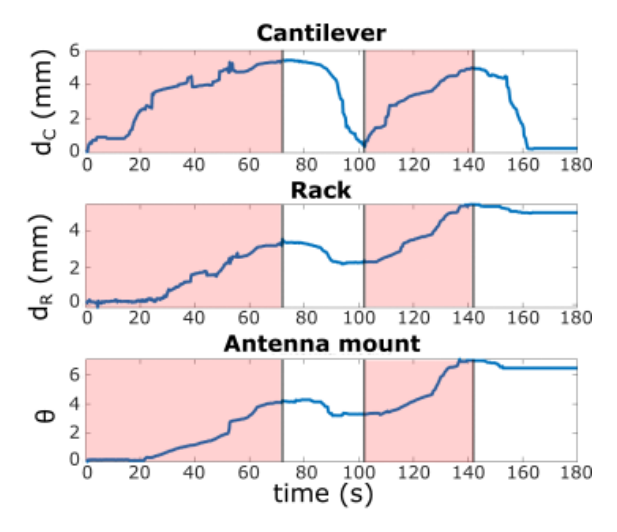


Fig. 8: The displacement of all moving parts of the inchworm mechanism in time. The linear displacements of the cantilever and the rack are shown in millimeters, and the rotational angle of the antenna mount in degrees. The red region indicates when the light is on. After the light is turned off, the rack and antenna mount remain stationary, meeting Requirement 4 from Table I.

by drawing the shape, heat seal lines, and alignment pin locations on heat sealable mylar with a pen on a Cricut 2D plotter. In addition, the heat absorbing fabric squares (0.75 in²) were cut in bulk on the Cricut to ensure uniform size. Then, a second layer of mylar was sealed to the first on 3 sides. The fabric squares were then inserted along with 0.05 mL of Novec 7000. Then the fourth side is sealed, excess material is trimmed off, and alignment holes are punched before attaching these to the array. This portion of the fabrication could be automated in the future.

V. EXPERIMENTAL RESULTS

In this section, we describe a series of experiments that characterize the behavior of the proposed individual actuator before describing tests of the full proof-of-concept array with 10 actuator units. Importantly, this section quantifies the system and confirms that Requirements 3-5 from Table I are met. (Requirements 1-2 were described in Section IV).

A. Single-cycle Heating and Cooling

The first set of experiments characterized the response of a single unit of the array during and after light irradiation. The light used was a 100 Watt infrared reptile basking spot lamp (Exo-Terra) and mounted 79 cm above the device. In order to prevent the lamp from heating multiple pouch motors, it was focused with two fresnel lenses (OpticLens) at 23 and 32 cm above the unit. The light and lenses were mounted to two linear actuators (ECO-WORTHY) that could move the light in X and Y over the entire array.

During irradiation, we tracked the displacement of the cantilever, the displacement of the rack, and the rotation of the antenna mount (Fig. 8). From this data, we see that the cantilever moves rapidly first, before engaging the rack and antenna mount, which only move significantly after approximately 15 seconds. All three then move together until

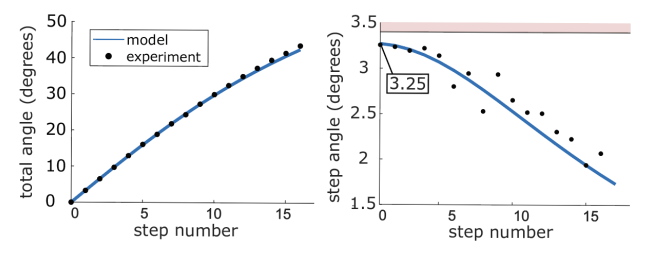


Fig. 9: The range and resolution of a single unit. The device can step 44 degrees with a worst case resolution of 3.25 degrees. This meets the requirements defined in Table I (40 degrees range and 3.4 degrees resolution).

around 75 seconds when the light is turned off. All three then move back slightly until the cantilever disengages with the rack, at which point the rack and antenna mount stop their motion. The cantilever then continues its motion until it is reset and ready for another cycle. During the second cycle, the actuation is much faster, due to the heat still in the pouch motor. In this cycle, actuation occurs in approximately 40 s.

B. Requirement 3: Large Range

The purpose of the next experiment was to determine if the fabricated device matched the required resolution and range from Requirement 3 of Table I. Specifically, we sought to test whether repeated motions of the cantilever would drive the rack to the end of its range, and whether each motion of the cantilever would move the rack the predicted amount. At the same time, we also sought to verify equation (1), which relates angular step size to rack position. This test was done by manually flexing the cantilever through its standard motion 16 times such that the rack advanced 16 steps.

The results of this test show that the desired one-direction range of greater than 40 degrees was achieved (Fig. 9). Further, the step resolution target of less than 3.4 degrees was also achieved, with every step under this value. Finally, our model from equation (1) matches well for both the total angle and step angle. Due to the geometry of the device, our angular resolution increases near the end range of the rack. Importantly, with these experiments, we confirmed that we were able to meet Requirement 3 from Table I.

C. Requirement 4: Position Retention

Critical to the design requirements is the ability for an antenna to remain steadily in one position for long periods of time, while a signal is being broadcast. Our design enables this by disengaging the cantilever from the rack, such that lengthening of the actuator during cooling does not move the rack. Fig. 8 shows that after the light is turned off, the rack and antenna mount stay stationary. The discrete design of the rack can accommodate overshoot in cantilever motion, if the rack has successfully advanced one tooth. During the heating cycle, the cantilever pushes the rack more than is required; but when the light is turned off, the cantilever pulls the rack back such that the total displacement is one tooth, thus satisfying Requirement 4, as shown in Fig. 8. The rack and antenna mount will continue to maintain their position until activated again with light.

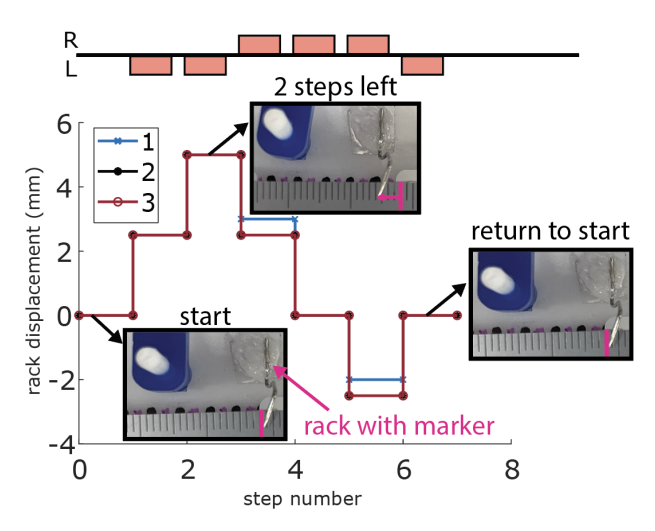


Fig. 10: A light actuated the unit to move to the left 2 steps (positive displacement), then to the right 3 steps (negative displacement), and finally, back to the left one more step to its initial position. The top shows the signal and the bottom shows the measured displacement. The first unit shows small, sub-millimeter error, while the other two showed no measurable error to within the nearest 0.5 mm.

D. Requirement 5: Accuracy, and Repeatability

To characterize the accuracy and repeatability of the proposed device, we tested three different single units moving through the same commanded pattern. For each, the light irradiated one side for two cycles, the opposite side for three cycles, and then the original side for one last cycle. The position of the rack was measured to the nearest 0.5 mm. The goal was to show that a unit would return to the starting position coming from either direction, and that all three units performed the same. The results of the test are shown in Fig. 10. All three units achieved the accuracy target of less than 1mm error for all movements. The first unit had two positions that were off by 0.5 mm, but importantly, these errors do not propagate. This is because with each new movement, the discrete nature of the cantilever-rack interaction ensures that the next motion is within 0.5 mm of the desired location, regardless of the last motion. Additionally, the other two units made all steps within 0.25 mm (250 micrometers) of the target. With this result, we confirmed meeting Requirement 5 from Table I.

E. Multi-unit Array Demonstration

Lastly, we selected an arbitrary pattern demonstrating the range of angles our device is capable of achieving. As shown in Fig. 11 a, each row is the same pattern, and the angles across the row from right to left are 0°, 10°(3 cycles), 20°(6 cycles), 30°(10 cycles), and 40°(13 cycles) where the number of steps are calculated with the angular resolution model (1), shown in Fig. 4, and rounded to the nearest whole number. Then, the same light setup from Sec. V-A was used to sequentially heat each pouch, scanning each row from right to left until the correct number of cycles were completed for each unit. After one unit is heated sufficiently, the next unit is heated and moved one step while the previous unit

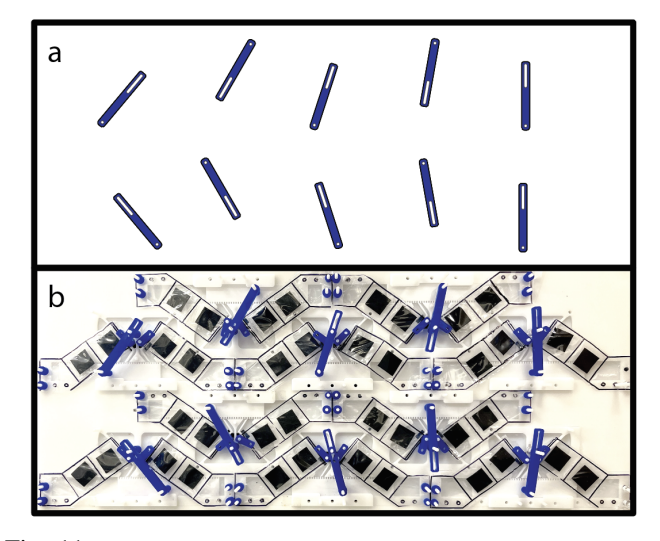


Fig. 11: A demonstration of patterning an arbitrary collection of antenna rotations across 10 different units of the array. a) is the planned pattern, and b) is the pattern reproduced on the array. See Fig. 1 for the starting pattern (all antenna holders vertical).

is still cooling, allowing actuation cycles to occur in parallel and decreasing the total time it takes to attain the desired configuration. Additional lights can also be added to this setup to heat multiple units simultaneously.

VI. CONCLUSIONS AND FUTURE WORK

We combined the high precision, accuracy, and position resolution of MEMS inchworm actuators with photothermal actuators, which are electronic- and metal-free in order to fabricate a device that can fulfill the design requirements (see Table I) for a mechanically reconfigurable diffraction-based antenna array. Future directions for this work could include scaling up the number of units from 10 to 100s, in order to match what is required for antenna arrays with multiple focal points. Scaling up the size creates challenges for the current automated light control X-Y gantry. Building a gantry at large scales is not ideal due to speed limitations, so a laser/mirror setup could instead be constructed. Additionally, scaling up requires an increase in actuation speed of the pouch motors, potentially by increasing the power of the light or using a more focused source, such as a laser. Finally, incorporating metal thin, light, metallic plates as antennas and testing the ability of the device to modulate EM signals is a key next step.

REFERENCES

- B. Han, Y.-L. Zhang, Q.-D. Chen, and H.-B. Sun, "Carbon-based photothermal actuators," *Advanced Functional Materials*, vol. 28, no. 40, p. 1802235, 2018.
- [2] J. Kim, J. W. Kim, H. C. Kim, L. Zhai, H.-U. Ko, and R. M. Muthoka, "Review of soft actuator materials," *International Journal of Precision Engineering and Manufacturing*, vol. 20, pp. 2221–2241, 2019.
- [3] C. J. Barrett, J.-i. Mamiya, K. G. Yager, and T. Ikeda, "Photo-mechanical effects in azobenzene-containing soft materials," *Soft Matter*, vol. 3, no. 10, pp. 1249–1261, 2007.
- [4] "The next hyper connected experience for all," Samsung's 6G White Paper, July 2020.
- [5] G. C. Alexandropoulos, N. Shlezinger, and P. Del Hougne, "Reconfigurable intelligent surfaces for rich scattering wireless communications: Recent experiments, challenges, and opportunities," *IEEE Communications Magazine*, vol. 59, no. 6, pp. 28–34, 2021.
- [6] M. Di Renzo, A. Zappone, M. Debbah, M.-S. Alouini, C. Yuen, J. De Rosny, and S. Tretyakov, "Smart radio environments empowered by reconfigurable intelligent surfaces: How it works, state of research, and the road ahead," *IEEE journal on selected areas in communica*tions, vol. 38, no. 11, pp. 2450–2525, 2020.
- [7] S. Gong, X. Lu, D. T. Hoang, D. Niyato, L. Shu, D. I. Kim, and Y.-C. Liang, "Toward smart wireless communications via intelligent reflecting surfaces: A contemporary survey," *IEEE Communications* Surveys & Tutorials, vol. 22, no. 4, pp. 2283–2314, 2020.
- [8] G. Gradoni, M. Di Renzo, A. Diaz-Rubio, S. Tretyakov, C. Caloz, Z. Peng, A. Alu, G. Lerosey, M. Fink, V. Galdi, et al., "Smart radio environments," arXiv preprint arXiv:2111.08676, 2021.
- [9] Q. Wu, S. Zhang, B. Zheng, C. You, and R. Zhang, "Intelligent reflecting surface-aided wireless communications: A tutorial," *IEEE Transactions on Communications*, vol. 69, no. 5, pp. 3313–3351, 2021.
- [10] E. Björnson, H. Wymeersch, B. Matthiesen, P. Popovski, L. Sanguinetti, and E. de Carvalho, "Reconfigurable intelligent surfaces: A signal processing perspective with wireless applications," *IEEE Signal Processing Magazine*, vol. 39, no. 2, pp. 135–158, 2022.
- [11] A. Pallaprolu, W. Hurst, S. Paul, and Y. Mostofi, "I beg to diffract: RF field programming with edges." ACM Digital Library.
- [12] T. J. White and D. J. Broer, "Programmable and adaptive mechanics with liquid crystal polymer networks and elastomers," *Nature materials*, vol. 14, no. 11, pp. 1087–1098, 2015.
- [13] H. Wermter and H. Finkelmann, "Liquid crystalline elastomers as artificial muscles," e-Polymers, vol. 1, no. 1, p. 013, 2001.
- [14] X. Lu, C. P. Ambulo, S. Wang, L. K. Rivera-Tarazona, H. Kim, K. Searles, and T. H. Ware, "4d-printing of photoswitchable actuators," *Angewandte Chemie International Edition*, vol. 60, no. 10, pp. 5536–5543, 2021.
- [15] H. Kim, J. A. Lee, C. P. Ambulo, H. B. Lee, S. H. Kim, V. V. Naik, C. S. Haines, A. E. Aliev, R. Ovalle-Robles, R. H. Baughman, et al., "Intelligently actuating liquid crystal elastomer-carbon nanotube composites," Advanced Functional Materials, vol. 29, no. 48, p. 1905063, 2019.
- [16] T. Hiraki, K. Nakahara, K. Narumi, R. Niiyama, N. Kida, N. Takamura, H. Okamoto, and Y. Kawahara, "Laser pouch motors: Selective and wireless activation of soft actuators by laser-powered liquid-to-gas phase change," *IEEE Robotics and Automation Letters*, vol. 5, no. 3, pp. 4180–4187, 2020.
- [17] R. Niiyama, X. Sun, C. Sung, B. An, D. Rus, and S. Kim, "Pouch motors: Printable soft actuators integrated with computational design," *Soft Robotics*, vol. 2, no. 2, pp. 59–70, 2015.
- [18] S. Iqbal and A. Malik, "A review on mems based micro displacement amplification mechanisms," *Sensors and Actuators A: Physical*, vol. 300, p. 111666, 2019.
- [19] J.-S. Park, L. L. Chu, A. D. Oliver, and Y. B. Gianchandani, "Bent-beam electrothermal actuators-part ii: Linear and rotary microengines," *Journal of Microelectromechanical systems*, vol. 10, no. 2, pp. 255–262, 2001.
- [20] J. Li, H. Huang, and T. Morita, "Stepping piezoelectric actuators with large working stroke for nano-positioning systems: A review," Sensors and Actuators A: Physical, vol. 292, pp. 39–51, 2019.
- [21] T. L. Bergman, F. P. Incropera, D. P. DeWitt, and A. S. Lavine, Fundamentals of Heat and Mass Transfer. Hoboken, New Jersey: Wiley, 2007.